DOI: 10.13009/EUCASS2019-290

Advanced methodologies for conceptual design of commercial aircraft empennages

Eduardo González Hernando, Fermín Navarro Medina**, J. Omar Martínez Lucci**, M. Ángel González Hernández****

**Future Projects Office, Airbus*

Paseo de John Lenon, 28906 Getafe, Spain, eduardo.g.gonzalez@airbus.com

***Department of Industrial and Aerospace Engineering, UEM*

Calle Tajo, 28670 Villaviciosa de Odón, Madrid, Spain, fermin.navarro@universidadeuropea.es and joseomar.martinez@universidadeuropea.es

****Wind Tunnel Facilities, ITER*

Polígono Industrial de Granadilla, 38600 Granadilla, Santa Cruz de Tenerife, Spain, ipviento@gmail.com

Abstract

This paper attempts to describe a methodology suitable for conceptual design of aircraft empennages. The workload was split in empennage concept downselection, empennage definition using Vortex-Lattice (AVL) as low fidelity method and Lattice-Boltzmann (XFlow) as high fidelity method, generation of an aerodynamic database with XFlow and validation in Wind Tunnel. Assessment between Wind Tunnel and XFlow data showed a good correlation, validating the use of XFlow for low speed aerodynamics of empennages in conceptual design. Airbus performed the empennage design, aerodynamic database generation and methodology validation. UEM and ITER performed the wind tunnel model design, manufacturing and testing.

Nomenclature

CAD	=	Computer Aided Design
CAM	=	Computer Aided Manufacturing
CFD	=	Computational Fluid Dynamics
C_m	=	Pitching moment
$C_{m\alpha}$	=	Pitching moment due to angle of attack
C_n	=	Yawing moment
$C_{n\beta}$	=	Yawing moment due to angle of sideslip
CNC	=	Computer Numerical Control
HTP	=	Horizontal Tail Plane
ISA	=	International Standard Atmosphere
ITER	=	Instituto Tecnológico y de Energías Renovables
MAC	=	Mean Aerodynamic Chord
Re	=	Reynolds number
SL	=	Sea Level
UEM	=	Universidad Europea de Madrid
V	=	Velocity
WTT	=	Wind Tunnel Test
α	=	Angle of attack
β	=	Angle of sideslip
ε	=	Mean downwash at empennage location
B	=	Body
N	=	Nacelle
T	=	Tails or Empennage
W	=	Wing

DOI: 10.13009/EUCASS2019-290

1. Introduction

It is known that decisions taken in the early phases of aircraft design have a large impact on the final product, leaving small freedom for changes in the rest of the design phases. Nevertheless, the resources required in those early phases are a small part of the total involved in the complete process. Thus, improving the methodologies used in preliminary design provides great benefits with a low investment, clearly justifying the research in this area.

Increasing computing and prototyping capabilities are beginning to allow the use, in the conceptual design, of highly demanding Computational Fluid Dynamics (CFD) methods for aerodynamic design and analysis as well as Rapid Prototyping techniques to manufacture models for aerodynamic testing and validation. As highly optimized commercial aircraft configurations leave little margin for improvement, exploring alternative concepts may open the way to further improvements in the aircraft performances.

The Future Projects Office of Airbus Operations, in collaboration with the department of Industrial and Aerospace Engineering of UEM and the Wind Tunnel Facilities of ITER, has accomplished the preliminary design of five empennage concepts; from the concept down-selection, through the computational design up to the test in wind tunnel, and the validation of the usage of methodologies commonly set aside for more mature design phases.

This report attempts to describe the methodology used for the preliminary design of aircraft empennages and the validation of the use of Lattice-Boltzmann methods for aerodynamic analysis in this design phase.

2. Conceptual and preliminary design of empennages

In the framework of the TAILS project, the main objectives were the exploration of different empennage concepts and the validation of advanced methodologies for the early phases in preliminary design.

In order to get a fair comparison of the aerodynamic behaviour among the different empennage concepts, a common target on longitudinal and lateral-directional stability is set. This requirement is established by the stability provided by the fuselage-mounted configuration (A-1 in Figure 1 from [1]), from now on the reference or conventional concept.

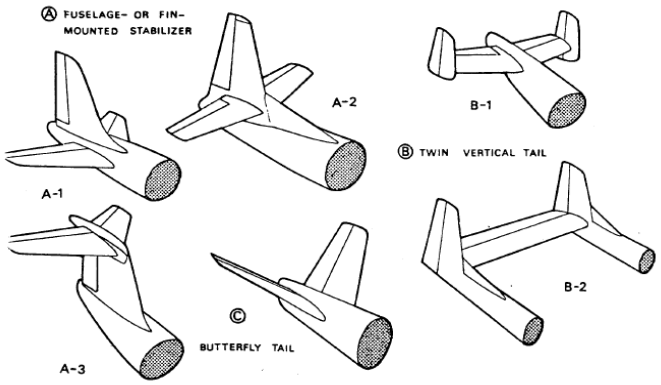

Figure 1 - Classification of Empennage concepts

The concept of natural stability refers to the ability of the aircraft to return to an attitude of equilibrium after a perturbation. In commercial aircrafts this function is generally provided by the empennage, which generates an aerodynamic force located aft of the aircraft centre of gravity. Thus, providing a restoring moment that allows the aircraft to be naturally stable.

The condition for natural static longitudinal stability is that the derivative of the pitching moment with respect to the angle of attack must be negative (according to the stability axis of Figure 2), i.e., a perturbation resulting in an increase in angle of attack generates a restoring pitching moment (nose-down). This derivative can be split into the wing-body and the empennage contribution as follows;

$$\frac{\partial C_m}{\partial \alpha} = C_{m\alpha} = C_{m\alpha}^{WB} + C_{m\alpha}^{T} < 0$$

Where C_m is the pitching moment, α is the angle of attack, *WB* refers to the wing-body and *T* refers to the empennage. Note that wing-body of commercial aircraft is usually unstable ($C_{m\alpha}^{WB} > 0$), mainly due to body contribution, requiring a stable empennage contribution (at least $C_{m\alpha}^{T} < -C_{m\alpha}^{WB}$).

DOI: 10.13009/EUCASS2019-290

The condition for natural static directional stability is that the derivative of the yawing moment with respect to the angle of sideslip must be positive (according to the stability axis of the Figure 2), i.e., a perturbation resulting in an increase in angle of sideslip generates a restoring yawing moment (nose aligning with the wind direction). This derivative can be split into the wing-body and the empennage contribution as follows;

$$\frac{\partial C_n}{\partial \beta} = C_{n\beta} = C_{n\beta}^{WB} + C_{n\beta}^{T} > 0$$

Where C_n is the yawing moment, β is the angle of sideslip, *WB* refers to the wing-body and *T* to the empennage. Note that the wing-body of a commercial aircraft is usually unstable ($C_{n\beta}^{WB} < 0$), mainly due to body contribution, requiring a stable empennage contribution (at least $C_{n\beta}^{T} > -C_{n\beta}^{WB}$).

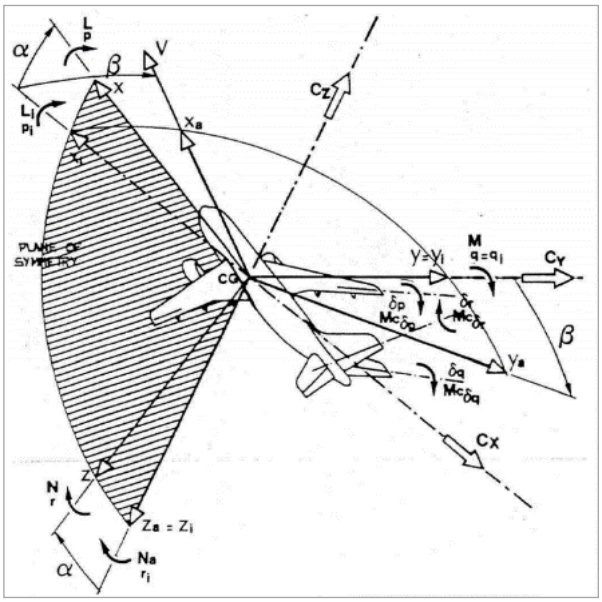

Figure 2 - Axis system

Dynamic stability is associated with both the angular velocities and the linear accelerations of the aircraft. In preliminary design, it can be assumed that these angular velocities and linear accelerations create a mean local angle of attack and sideslip at the empennage location only dependant on the empennage distance to the aircraft centre of rotation and on the wing-body downwash and sidewash [2]. Thus, the contribution of the empennage to the dynamic stability of the aircraft is directly proportional to its contribution to the static stability. This allows the reduction of the targets to only the static criteria, by assuming the reference empennage is well sized for both static and dynamic criteria, thus the rest of empennages will be well sized as long as they meet the targets for static criteria.

Controllability, manoeuvrability and trim requirements are not covered in this study. Therefore, there is no control surface definition for any of the empennage configurations studied. Further studies could cover this topic in a similar approach than the one followed in this study.

Therefore, the constraints imposed to the design of the different empennage configurations are as follows;

$$C_{m\alpha}^{T} \leq C_{m\alpha_{target}}^{T} = C_{m\alpha}^{Tconventional} \qquad \& \qquad C_{n\beta}^{T} \geq C_{n\beta_{target}}^{T} = C_{n\beta}^{Tconventional}$$

During the initial phase of exploration of empennage concepts a down-selection was carried out, to reduce the design space to a number of concepts according to the time constraints of the TAILS project, roughly one year. Five concepts were selected: Conventional tail, Cross-tail, T-tail, U-tail and V-tail, with the last three ones with and without engines mounted at the rear-fuselage. All of these empennage concepts were mounted in a classical wing-body with low-wing.

Figure 3 - Empennage concept down-selection

Empennage sizing and definition was performed in an iterative cycle, using Vortex-Lattice methods (AVL) as low fidelity and Lattice-Boltzmann methods (commercial software XFlow) as high fidelity. On the one hand, low fidelity methods have a low computational cost and estimate the linear behaviour of lifting surfaces with the sufficient accuracy to enable empennage sizing and planform optimization loops in the presence of a wing. On the other hand, results from high fidelity methods were used to correct the low fidelity methods where there is a notable lack of accuracy, i.e., fuselage bodies or detached flow in lifting surfaces at high angle of attack, thus improving the accuracy in the optimization loops. For those concepts with the option of the engines at the back, the engine contribution to stability was not taken into account for the empennage sizing. Note that engines were simulated as flow-through nacelles.

DOI: 10.13009/EUCASS2019-290

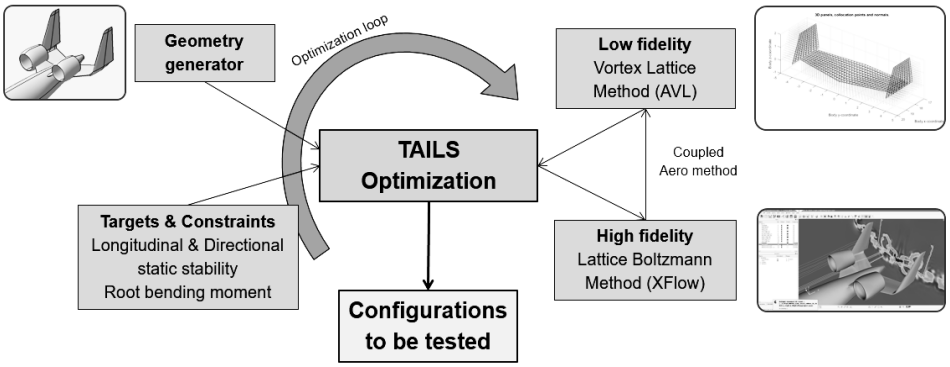

Figure 4 - Empennage design workflow

Validation of this computational empennage sizing and definition, for all of the previous concepts, was carried out with a low-speed wind tunnel test campaign. In addition, tests done in the wind tunnel were replicated with XFlow to validate this high fidelity method.

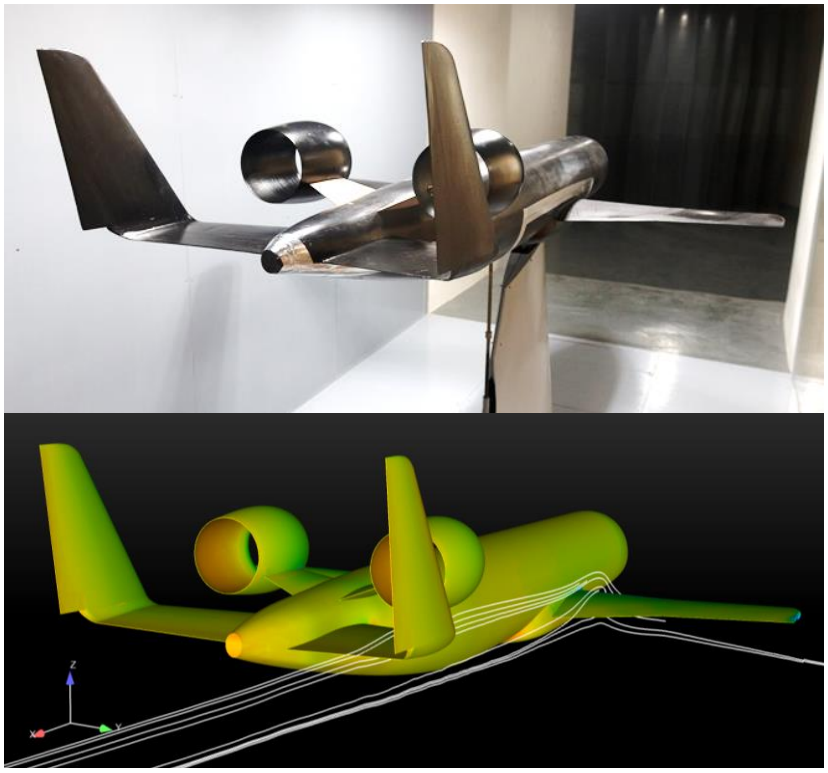

Figure 5 - U-Tail concept with nacelles - WTT vs CFD

3. Equivalent wing for wind tunnel

Aiming to evaluate the empennage characteristics in a wind tunnel test, a wing with reduced span providing an equivalent downwash at empennage location was designed to maximize the wind tunnel model scale. The new wing was designed according to the methodology described in [3], in which is stated that an equivalent flow field at empennage location is ensured as long as the wing load distribution is replicated up to a wing span location that covers the whole span of the empennage. For that, chord and twist laws of the wing are modified to match both the basic and the additional wing lift distributions in the required wing-span.

The methodology was applied to an isolated wing in a Vortex Lattice Method (AVL) and the resulting wing was checked with a Lattice Boltzmann Method (XFlow) in a wing-body configuration.

DOI: 10.13009/EUCASS2019-290

The design of the wing with reduced span, for the aircraft with the conventional empennage, revealed that a 35% of wing span reduction is achievable without changing the inner wing load distribution in a length covering the empennage span. This reduction allows an increase model scale of approximately a 50%, which leads to the same increase in Reynolds number. Figures 6 and 7, obtained with AVL, demonstrate the previous statement:

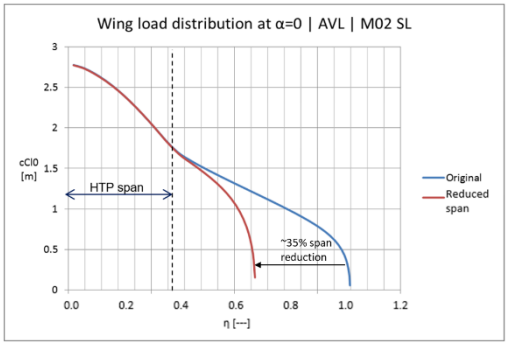

Figure 6 - AVL wing load distribution at alfa 0

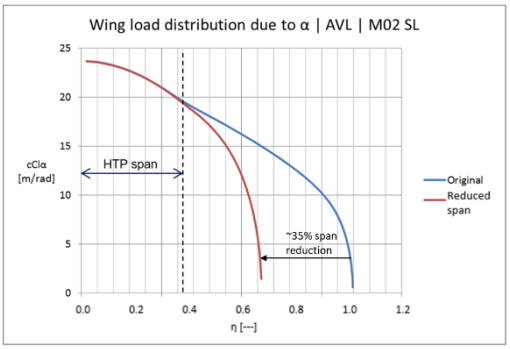

Figure 7 - AVL wing load distribution due to alfa

Wing load distributions have been checked with XFlow, confirming the AVL results. Moreover, flow fields as the local angle of attack and the local dynamic pressure, also from XFlow results, were monitored at the empennage location (x-location of 25% of MAC of reference HTP). Differences between the flow fields of the original wing and the reduced-span wing are shown in the following figures:

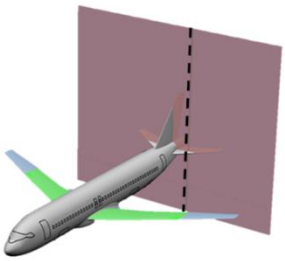

Figure 8 - Empennage plane for monitoring

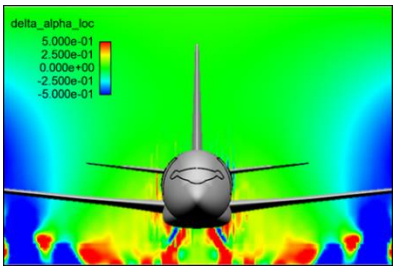

Figure 9 - Differences in local angle of attack at α=5º (Original minus Reduced-span, range ±0.5º)

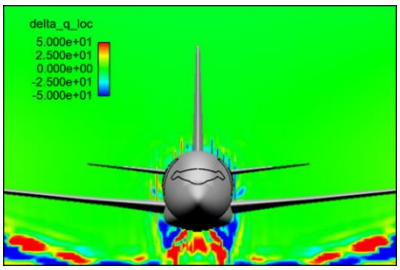

Figure 10 - Differences in local dynamic pressure at α=0º and α=5º (Original minus Reduced-span, range ±50Pa)

Green regions mean no difference between flow fields. Therefore, it is assessed that flow conditions at empennage location are equivalent with both the original and the reduced-span wing and a 50% of model scale is achievable with this strategy.

4. CFD aerodynamic database generation

An aerodynamic database, defined in accordance with the tests to be performed in the wind tunnel and the time constraints of TAILS the project, was generated using CFD with Lattice Boltzmann Method (XFlow). For that, each empennage concept was computed at the wind tunnel conditions; V=48m/s, SL, ISA+15, in a complete α-polar up to the positive stall with null sideslip to evaluate the longitudinal stability (6 α-breakpoints in the range α=[+0º,+14º] with β=0º) and in an α-β-matrix to evaluate the directional stability at low angle of attack (4 α-β-breakpoints in the range α=[+0º,+5º] and β=[+5º,+10º]), summing up a total of 10 cases per configuration. In addition, it was decided to split up each concept in several combinations of the components: wing, body, tail and nacelles, in order to identify better the different contributions to the aircraft stability and the potential interferences among them (i.e., downwash at empennage location), leading to a total of 18 configurations as shown in the Figure 11.

DOI: 10.13009/EUCASS2019-290

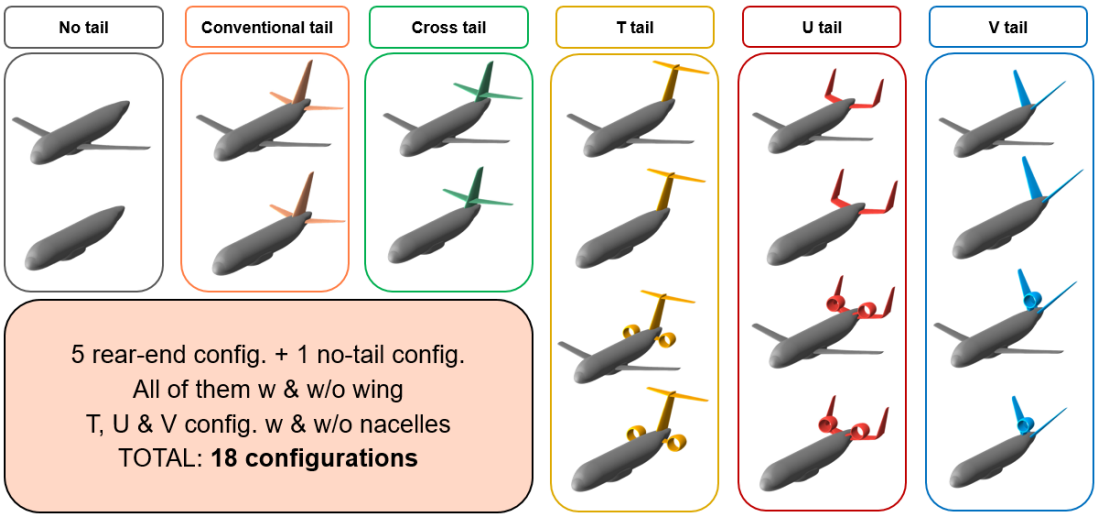

Figure 11 - Concept and component breakdown

Mesh sensitivity studies were carried out to determine the best trade between computational time and the required accuracy in preliminary design, again bearing in mind the time constraints of the TAILS project. The mesh generated for the calculations was a Cartesian multi-block mesh composed of 11 levels in a square domain of 240 chords in each direction, with a smallest size cell of 1 mm and refinement boxes of 4 mm cell size in the wake of the wing to capture the flow conditions at empennage location, leading to a total number of elements of around 60 million in the worst case scenario of a wing-body-tail-nacelle configuration. The turbulence model selected was a wall-adapting local-eddy model with a non-equilibrium enhanced wall-function.

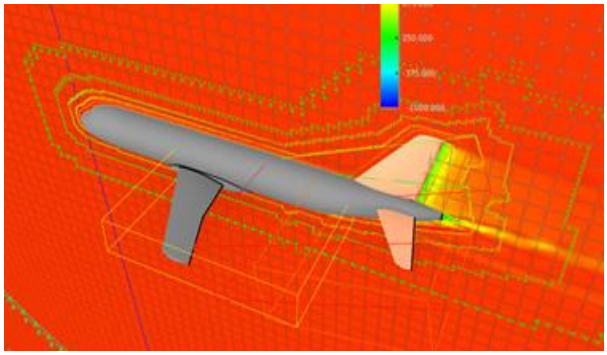

Figure 12 - CFD mesh

In total, 18 configurations each at 10 flight conditions with a mesh of 60 million of elements, leading to 180 cases with a total computing time of nearly 1 month non-stop.

Analysis of the computed data confirmed the estimations of the static stability of the aircraft, done in the phase of the design of the different empennage concepts, with a maximum deviation of ±5% for both $C_{m\alpha}$ and $C_{n\beta}$ of the different empennage concepts with respect the conventional empennage.

5. Model description

In this section, the test model design is described and the technical decisions for the model breakdown are argued. The selection of scale model, the material and the manufacturing process including the milling campaign description and an estimation of structural rigidity and strength of wings has been included.

Both the test model design and manufacturing were performed at UEM facilities (Villaviciosa de Odón, Spain). The first step in the test model design was the selection of model scale, taking into account a 35% of wing span reduction of the model. To select it, several criteria have been evaluated. First, cross-section blockage of wind tunnel was evaluated, up to angles of attack of 25º, leading to an upper limit of the model scale of 1:15. Second, it is recommended to place the model in the constant cross section of the wind tunnel, thus limiting the longitudinal distance between the wing and the rear-end to 1.4 m, leading again to an upper limit of the model scale of around 1:15. Lastly, the larger the model scale the larger the Reynolds number, improving the fidelity of the test. From all these factors, a model scale of 1:15 was chosen.

The final decision of the material and manufacturing processes was taken on an overall compromise among mechanical properties, surface quality, manufacturing capabilities and costs. According to that, it was decided that the test models were going to be manufactured by milling beech wood. For this reason and taking into account the dimensions of beech

DOI: 10.13009/EUCASS2019-290

boards and especially their thickness, it was decided to split the models into sections and subsections for a simpler and more manageable construction. Moreover, a modular wind tunnel model was designed to reduce the costs of the wind tunnel tests, allowing a rapid interchanging of the components to minimize the time spent in the set-up of the different configurations to be tested. In Figure 13, it can be observed the design of the modular model; on the left-hand side the body with and without the wing-belly, on the right-hand side the empennage support with two empennage concepts.

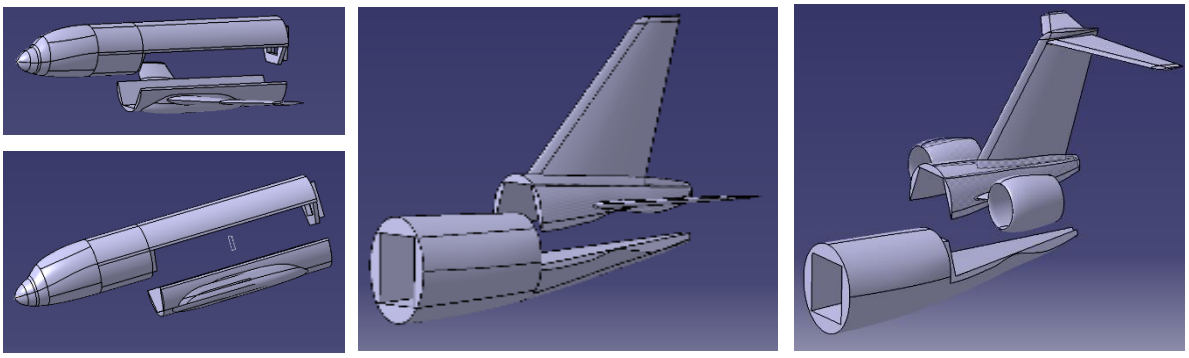

Figure 13 – Samples of modular test model parts

An advanced Computer-aided manufacturing (CAM) software was used to define the operations for the manufacturing process of the aircraft model. The software provided the computer code to be uploaded in a 3-axis CNC milling machine. To accomplish the manufacturing of the model, it was necessary to implement it in three principal phases: the preparation of the raw material, the roughness milling and the finishing process.

The first phase was to prepare the block of the beech board to be milled. In the case of small thickness pieces, the preparation was straightforward. In the case of pieces with higher thickness than the raw wood, the preparation was to bond two or more blocks boards to reach the desirable part dimension. The design of the test model is highly dependent on the milling process. To improve the accuracy of the final geometry pieces are required to have a planar face, so that the mill can be positioned only once over the milling machine table. Moreover, the impossibility of access for the 3-axis mill for angles higher than 180º, with respect to the upward vertical direction, imposes the need of convex surfaces. Finally, the milling machine is limited up to 120mm at vertical-axis, forcing to split the parts with higher thickness into small pieces, then joining all the pieces together with adhesives of screws. For parts with one planar face, as the fuselage, it was only necessary to mill one side of the pieces. Nevertheless, wing and tails were manufactured in one piece due to aerodynamic requirements for the leading edge, requiring milling both the upper and lower surfaces. Therefore, tabs were placed on the lateral sides of the piece in order to ensure the correct positioning when the board was turned to mill the other surface. Figure 14 shows the two different types of milling processes: on top, a fuselage part that only needs to be milled by one side; on the bottom, a wing part that needs to be milled both sides.

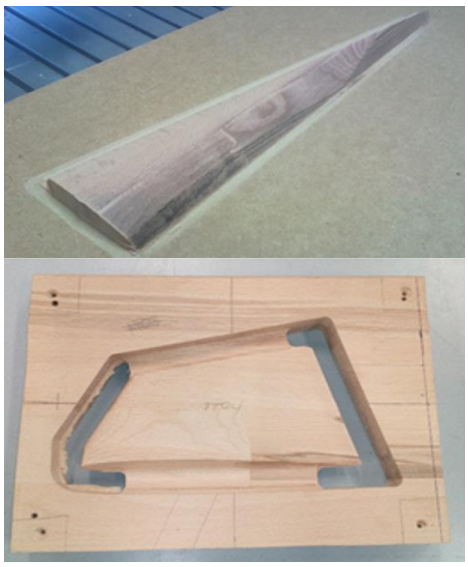

Figure 14 - Piece milled, only at one side (top) and piece milled both sides with lateral tabs (bottom)

Due to the limitations of thickness of beech wood planks, it was decided to divide the fuselage into 5 different longitudinal sections, and each of these sections into 4 or 6 cross-sectional pieces. Besides, transversal reinforcements were included to better withstand shear forces on the fuselage and L-shaped reinforcements were screwed to the joints between pieces to ensure the resistance of the junctions. It should be remarked that the needed thickness for manufacturing one-plane-side pieces in some sections is thicker due to the fuselage cross-section variation. Thus, the glue of two planks and the milling in a single piece to achieve the desired thickness has been designed when needed. A comparison of a manufactured and CAD model of a section of the fuselage is shown in Figure 15.

DOI: 10.13009/EUCASS2019-290

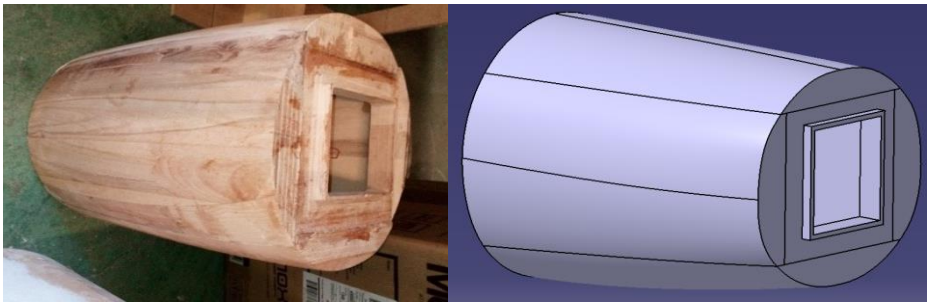

Figure 15 - Manufactured (left) and CAD model (right) of a section of the fuselage

The second phase was to perform the roughing milling. A 10-mm-diameter milling tool was used, leaving a margin of 0.3 to 0.5 mm on the surface to allow for the finishing process. A contour cut was performed to separate the parts from the raw wood. At this phase the same milling tool was used.

Finally, for the finishing process a hemispherical 8-mm-diameter milling tool was used. A final surface finishing treatment was performed to improve the surface roughness of the model. Treatment consisted on caulking, painting, sanding, and varnishing. The measurement of surface roughness was $0{,}2x10^{-6}$m, which agrees with the standard of models.

To prevent measurement errors during the wind tunnel test, it is desirable to place the support of the force balance as close to the model's center of gravity as possible, to reduce the effect of imbalanced forces. Considering the scale 1:15 and the density of wood is 0.9 g/cm^3, a first estimation of the weight and the location of the centre of gravity resulted on 73 kg and x=1046 mm, respectively. As the front support is located at x=1230 mm, the addition of lumped masses is placed in the interior of the fuselage to move the center of mass near the support.

To prevent any failure of the aircraft model during the wind tunnel test, it was necessary to perform different material tests in order to determine its mechanical properties. Flexural test, shear stress tests and tensile stress tests of the beech wood, as well as pulling tests of the screws, were performed in the UEM labs. The testing machine is SERVOSIS with a maximum force of 20 Tons in compression and tension. This force was sufficient to break the specimens to be tested. The testing speed of the load rate was constant, as required by the test specification and directions of the standards.

From these structural analysis it was concluded that the rigidity and strength of beech wood is enough to resist the critical loads expected in the wind tunnel. The maximum wing tip vertical displacement was estimated to be 2% of wing thickness and the expected direct stress due to bending moment was 1.05 MPa, far lower than the strength of the beech bar found in the flexural tests. The rest of structural tests gave an idea of the strength of junctions by screwing and gluing. To reinforce the internal structure a longitudinal metallic bar was placed embedded in additional transverse frames.

The inspection methods used to analyze the external surfaces of the manufactured model has been: hand-made measuring by ruler and calliper and scanner roughness by microscopic photography. A global analysis of the geometrical shape of the test models was done with a FARO laser scanner. Six scans around the model were taken, and merged into a single point cloud with SCENE, by using four white 15cm-diameter spheres as merging references. The combined point cloud was exported to CATIA, where the comparison with the original test model was done. To provide a general view of both the original and manufactured test models simultaneously, pictures of separated and superposed models are shown in Figure 16.

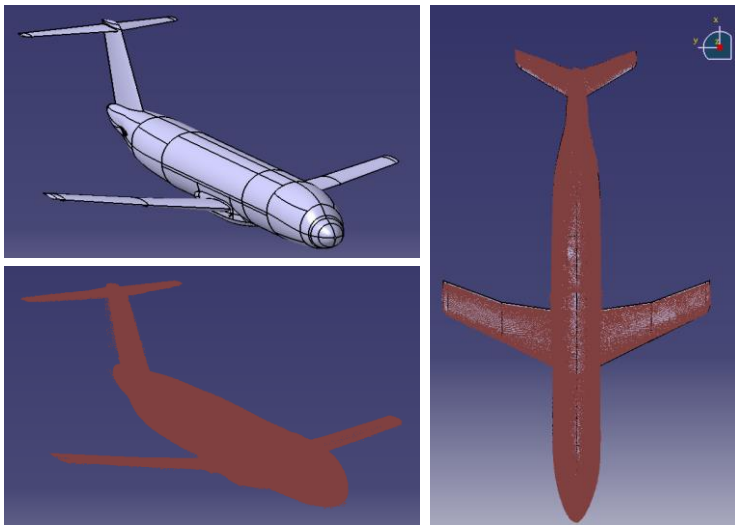

Figure 16 - CAD test model (top-left), cloud of points of manufactured model (bottom-left), and superposition of CAD and manufactured models (right).

DOI: 10.13009/EUCASS2019-290

6. Wind tunnel tests

Wind tunnel tests have been performed at the ITER facilities in Tenerife (Canary Islands, Spain). The ITER wind tunnel is a closed circuit, with closed test section. It is 3 m long with a 2x2 m^2 cross section. The maximum speed in aeronautic configuration (less than 0.5% turbulence level and flow uniformity better than 99.5%) is 48 m/s. In the standard configuration, used in these tests, the maximum speed is 56 m/s, with a uniformity above 98% and a turbulence level below 2%.

Figure 17 - V-tail visualization

The instrumentation used in this test campaign was an in-house design and build, six-component force balance. Drag is measured with a 500N-0.02% maximum error load cell, giving an absolute error of 0.1N. For a reference dynamic pressure of 1500 Pa and a reference area of 0.5m2, this leads to a 1 drag count error in drag coefficient. Lift is measured with the 3 vertical load cells. Taking into account range and maximum error of each load cell, the maximum expected error in lift coefficient measurement is 10 counts. Both errors correspond to static measurements. In order to keep these values in dynamic conditions, the sampling speed is 5 kHz. A hot wire anemometer and a Pitot tube measure the flow speed at the test chamber; local temperature and humidity are measured too.

Figure 18 - V-tail visualization (detail)

Once the model is mounted on the balance support, the beta angle is settled manually; meanwhile, a servomotor automatically controls the angle of attack. The measurement of each angle of attack lasts 10 seconds, while a period of 5 seconds is used to change the angle of attack, and a period of 10 seconds is waited for the wind tunnel flow to be stabilized.

Figure 19 - T-tail visualization

For a better understanding of the behaviour of the different concepts, some visualization tests were performed as well. A mixture prepared with talcum powder and petroleum was used to visualize the flow just in the model surface. Figures 17, 18 and 19 are shown to illustrate the visualization results.

The wind tunnel force measuring tests results are shown in the next chapter, in comparison with the CFD results.

7. CFD vs WTT comparison

Once the data from the WTT was obtained, a comparison between the CFD calculations and the WTT data was made, aiming to identify the strengths and weaknesses of the use of Lattice-Boltzmann CFD in preliminary design of empennages.

Due to confidentiality, scales have been removed from figures. Nevertheless, scales are the same across all related figures (i.e. all downwash figures), ensuring consistency and allowing to demonstrate the validity of the process.

DOI: 10.13009/EUCASS2019-290

Starting with the drawbacks, it was noticed that there are notable differences in the results of the isolated body, as shown in Figure 20 (body as light blue and light red, against wing-body or body-tail in dark blue and dark red). These differences in body lift and body pitching moment can be neglected when compared against to the wing lift and to the empennage pitching moment respectively. It was also noticed, that prediction of wing stall is not well matched. On the other hand, as the fuselage is a great contributor of the total drag of the aircraft, the differences in drag cannot be neglected, as shown in Figure 20 (bottom) where the differences are around 50 drag counts. In conclusion, it seems that XFlow is not very suitable for dealing with behaviors strongly related with the viscous contribution, such as the forces and moments of a fuselage, the stall of a lifting surface or drag in general.

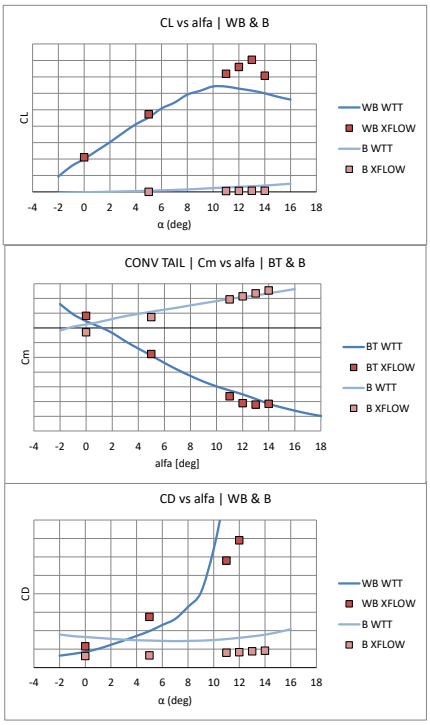

Figure 20 - Body assessment against wing-body (lift and drag) and body-tail (pitch). Lift, pitch and drag (from top to bottom).

Bearing in mind the previous issues, the contribution of the empennage to aircraft stability was evaluated both in absence and presence of the wing, with the contribution of the fuselage subtracted. That is, body-tail minus body and wing-body-tail minus wing-body, respectively. The differences between the previous contributions come from the so-called wing mean downwash at empennage location, which relates the angle of attack at the empennage location with the angle of attack upstream: $\alpha_T = \alpha - \varepsilon$. In absence of a wing, null downwash can be assumed. Thus, downwash can be estimated with both the WTT and the CFD results comparing the data as follows:

$$C_m^{BT} - C_m^{B} = f(\alpha = \alpha_T)$$

$$C_m^{WBT} - C_m^{WB} = f(\alpha = \alpha_T + \varepsilon)$$

The WTT and CFD data was treated according to the previous explanation and compared in Figures 21 and 22, showing that both the empennage contribution to pitching moment in presence of the wing-body and the wing downwash at the empennage location are captured well by XFlow (WTT as reference), for the different empennage concepts.

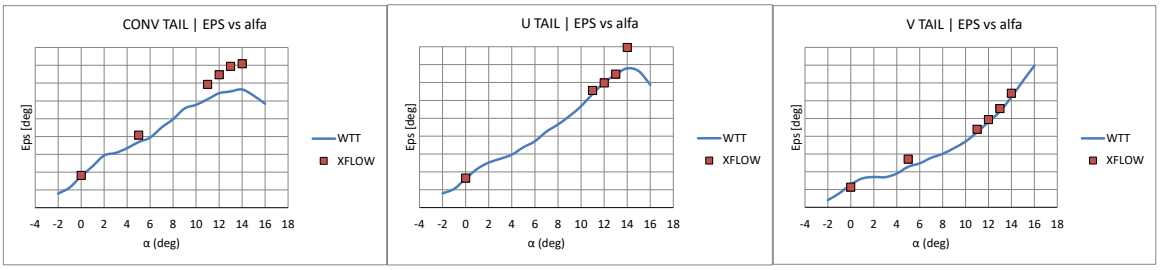

Figure 21 - Wing downwash at empennage location

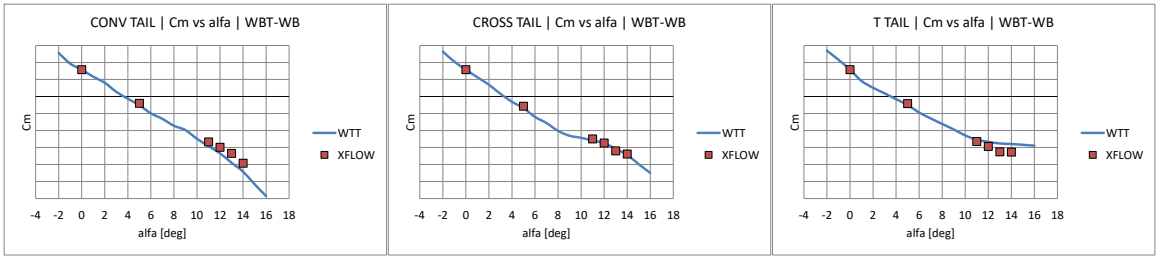

Figure 22 - Empennage contribution to pitching moment in presence of the wing-body

Note that the downwash at high angles of attack is not captured well due to the differences identified previously in the wing stall.

DOI: 10.13009/EUCASS2019-290

The contribution of the nacelles to longitudinal stability were processed in a similar manner, as shown in Figures 23 and 24. The nacelle contribution to pitching moment in the presence of the wing-body and the wing downwash at the nacelle location are captured well by XFlow (WTT as reference), for the different nacelle configurations.

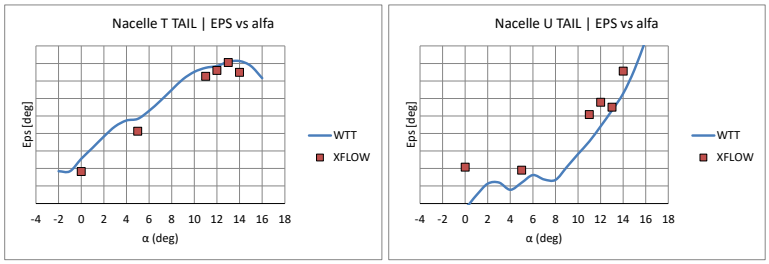

Figure 23 - Wing downwash at nacelle location

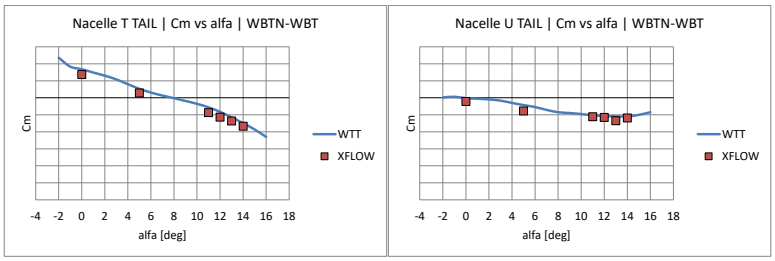

Figure 24 - Nacelle empennage contribution to pitching moment in presence of the wing-body

The same procedure was applied for directional stability leading to similar results. For instance, the conventional empennage contribution to yawing moment, in the presence and absence of the wing-body, is well captured using XFlow (WTT as reference) as shown in the Figure 25.

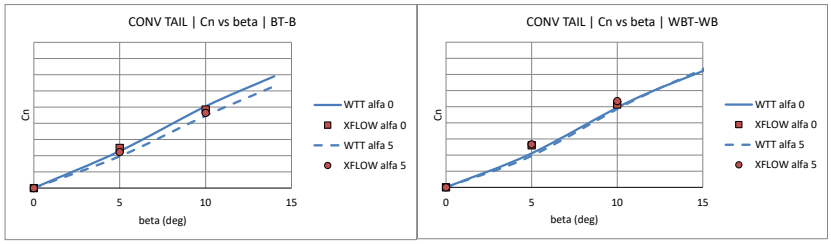

Figure 25 – Conventional empennage contribution to yawing moment

In conclusion, Lattice-Boltzmann CFD is suitable for estimating contribution of empennage and nacelles (at the rear-fuselage) to aircraft stability, in both the presence and absence of the wing-body, for preliminary design.

8. Conclusions

Conceptual and preliminary design of commercial aircraft empennages has been successfully accomplished by using a coupled methodology with Vortex-Lattice methods (AVL) as low fidelity and Lattice-Boltzmann methods (XFlow) as high fidelity. A wind tunnel test campaign has been carried out to validate the methodology, showing an accurate correlation with CFD data of empennage and nacelle contribution to aircraft stability.

It has been demonstrated the suitable of this process in terms of capability to cover a wide design space, reduced time consumption and accuracy of results.

Acknowledgments

This work was made possible through an efficient collaboration between industry and university; Airbus, UEM, ITER and the support of Clean Sky 2 WP1.2. The empennages and equivalent wing design, aerodynamic database generation and method validation were performed by Airbus. The wind tunnel model design and manufacturing was performed by UEM. The wind tunnel testing was performed by ITER.

DOI: 10.13009/EUCASS2019-290

We would like to thank the UEM and ITER teams for their proactive and close collaboration which made possible the manufacturing and wind tunnel testing of a low-cost multi-configuration model specifically prepared for preliminary design purposes.

References

[1] "Synthesis of Subsonic Airplane Design", Egbert Torenbeek, Springer, 1982
[2] "USAF Stability and Control Datcom", Douglas Aircraft Company Inc., 1960
[3] "Wind Tunnel Aircraft Model with Truncated Wing" US 8453964 B2, Esteban Amo Garrido, Pilar Vela Orge, Angel Pascual Fuertes, 4 Jun 2013
[4] "AVL (Athena Vortex Lattice) 3.36", Mark Drela, MIT Aero & Astro, 2017
[5] "Airplane Flight Dynamics and Automatic Flight Controls", Jan Roskam, The University of Kansas, 1979
[6] "Aircraft Design: A Conceptual Approach", Daniel P. Raymer, Conceptual Research Corporation, 1992
[7] "A Joint DLR-ONERA Contribution to CFD-based Investigations of Unconventional Empennages for Future Civil Transport Aircraft", Gerald Carrier, Lutz Gebhardt, Onera, DLR
[8] "Installed tailplane lift-curve slope at subsonic speeds", ESDU 89029, 1989
[9] "Average downwash at tailplane at low angles of attack and subsonic speeds", ESDU 80020, 1980
[10] "Pitching moment and lift force derivative due to rate of pitch for aircraft at subsonic speeds", ESDU 90010, 1990
[11] "Contribution of fin to sideforce, yawing moment and rolling moment derivatives due to sideslip, in the presence of body, wing and tailplane", ESDU 82010, 1982
[12] "Contribution of fin to sideforece, yawing moment and rolling moment derivatives due to rate of yaw", ESDU 82017, 1982